Stabilization of 2D graphene, functionalized graphene, and Ti_2CO_2 (MXene) in super-critical CO_2: A molecular dynamics study

[*]Rasoul Khaledialidusti[1], Ehsan Mahdavi[1, 2], Afrooz Barnoush[1]

[1]Department of Mechanical and industrial Engineering, Norwegian University of Science and Technology (NTNU), 7491 Trondheim, Norway.
[2]School of Mechanical Engineering, College of Engineering, University of Tehran, Tehran, Iran.

Abstract

The stabilization of nanoparticles is a main concern to produce an efficient nanofluid. Here, we carry out Molecular Dynamics (MD) modeling to evaluate the stabilization of 2D graphene, oxygen- and hydrogen- functionalized graphene, and Ti_2CO_2 MXene nano-sheets in carbon dioxide (CO_2) liquid at a supercritical condition. The rheological properties (i.e., viscosity and self-diffusion) of the nanofluids with the corresponding nano-sheets are also calculated. The results show that pristine graphene aggregate in the liquid and the adsorbed CO_2 molecules on the graphene surfaces could not provide enough repulsive forces to avoid their aggregation. The stabilization of graphene is improved by surface functionalization of graphene with oxygen and hydrogen functional groups. This is because, first, the presence of the corresponding surface groups can alter the electrostatic forces of the graphene nano-sheets and, second, a larger number of CO_2 molecules attracted by the functionalized nano-sheets can provide additional repulsive forces between the nano-sheets. The results demonstrate that Ti_2CO_2 MXene nano-sheets aggregate severely while they are covered by oxygen surface terminations and are attracted more CO_2 molecules than the pristine graphene. It is attributed to the strong interlayer coupling between the MXene nano-sheets so do that the electrostatic repulsion of the MXene surfaces could not overcome the interlayer coupling. Based on our results, the stabilization of the corresponding 2D nano-sheets in CO_2 liquid are in the order of: oxygen-functionalized graphene > hydrogen-functionalized graphene > pristine graphene > Ti_2CO_2 MXene. The calculation of the rheological properties of the nanofluids with different nano-sheets demonstrates that immersing the nano-sheets in the CO_2 liquid afford a superior

viscosity enhancement as much as they could disperse in the liquid. This study expand the potential applications of these 2D materials in producing SC-CO_2 based nanofluid.

1. Introduction

Nanofluids (NFs) have recently attracted much scientific attention due to their strengthening thermo-physical, chemical, rheological, and physiochemical fluid properties. Nanofluids are designed by dispersing nanometer-sized particles, named nanoparticles (NPs), to a base fluid. The suspension of nanoparticles in a base fluid would enhance the fluid properties, which have led nanofluids to be extensively studied for diverse applications in lubrication [1–4], oil and gas [5,6], chemical industries [7], and etc. The viscosity enhancement of the base fluids by dispersing nanoparticles were evaluated in many studies [8–13]. Although different works were performed for the simulation of nanofluids, most of them were studied the nanoparticle dispersion in an inert fluid (i.e., Argon) or water. The results of these studies show that the viscosity of the base fluids could be enhanced up to three times depending on the nanoparticle size and material, volume fraction, and thermodynamic conditions [8-10]. From these studies [8-13], it could be generally understood that smaller nanoparticles have a greater impact on the viscosity enhancement of the base fluids. Volume fraction of the nanoparticles is another important factor that has a significant impact on the viscosity enhancement of the base fluids. In industrial application, nanofluids are produced with the volume fraction of the nanoparticles in a range of between 1% to 4% [8]. From the literature [8-13], it could be understood that the viscosity enhancement of the base fluid have a direct relation with the volume fraction of the nanoparticles so that it enhances more significantly by increasing the volume fraction of the nanoparticles. It worth nothing that higher volume fraction of the nanoparticles would intense the problem of the nanoparticles aggregation in the solution. The proficiency of nanoparticles in improving the base fluid viscosity motivated us to bring this technology to a CO_2 injection

method in oil industry as an Enhanced Oil Recovery (EOR) method or CO_2 sequestration, which suffers from the low viscosity of the base fluid.

CO_2 injection method is widely studied and applied in oil industry either for EOR purposes by improving the displacement efficiency [14–16] or for sequestrating in oil formations [17]. However, it is well documented that this injection method might be break down due to the unfavorable viscosity of the CO_2 liquid [18–20]. For CO_2 miscible displacement at reservoir conditions, the viscosity of CO_2 is estimated to be in the range of 0.03 and 0.08 cP, which causes fingering of the CO_2 through the reservoir formation due to frontal instability and resulting inefficient oil production [20]. To overcome this weakness, the CO_2 viscosity enhancement was proposed by adding surfactant to the injecting fluid which provide a better sweep efficiency by stabilizing viscous fingering [18–21]. Although surfactant induces CO_2 foam and reduces CO_2 mobility, long-term stability of the CO_2 foam is an unfavorable issue especially at high temperature and high salinity reservoir environments. At higher temperatures, surfactants largely degrade and loss in the reservoirs by adsorption on the rock surface, which results in a large consumption of chemicals in CO_2 foam flooding, and thus limits the economic viability of this method.

It is recently addressed that new developments in nanotechnology would provide a condition for a better stabilization of CO_2 foam for months or even years [6,22–24]. Adding the nanoparticles to the super-critical (SC) CO_2 not only could enhance the CO_2 fluid viscosity, it could increase the foam stability more than surfactants as well. The main concern on immersing the nanoparticles in a fluid is the aggregation of the nanoparticles, which could reduce the functionality of the nanoparticles and block the low permeable pores in the case of oil industry application. In our previously published studies [6], we investigated the effect of a single CuO and Al_2O_3 NP on the viscosity enhancement of the SC-CO_2 liquid using Molecular Dynamics (MD) modeling. The results showed that the nanoparticle suspension in the SC-CO_2 could significantly enhance the rheological properties of the fluid, depending on the thermodynamic

conditions, volume fraction, the nanoparticle type and size as well as the nanoparticle shape. The stability of a nanofluid is associated to the clustering and aggregation of the nanoparticles, which is not feasible to be addressed using a single nanoparticle. Thus, in this study, we investigate the stabilization of 2D nano-sheets of graphene and newly developed Ti_2CO_2 MXene in CO_2 liquid using MD modeling. We also further investigate the stabilization of two-sided oxygen- and hydrogen-functionalized graphene with the functional group concentration of 50% in the CO_2 liquid in order to highlight the effect of the surface terminations on the problem. The enhancement of the rheological properties of the CO_2 liquid based nanofluid with the corresponding nano-sheets are also evaluated.

Graphene has been provided a wide range of opportunities in different applications and has extensively been studied due to its special properties including flexibility, chemical stability, mechanical properties, and molecule adsorption [25–28]. It has widely been accepted that functionalized graphene could further improve the most properties and applications of bare graphene [29,30]. For example, a graphene sheet is impermeable to molecules and to achieve permeability, drilled holes in the perfect graphene sheet are essential. There are two fields of application for the nanoporous graphene: (a) gas separation, (b) water purification. The functionalized nanoporous graphene can control the separation of molecules from a solution [31,32]. The other example is associated to the stabilization of graphene. The stabilization of functionalized graphene in different base fluids have been studied [31,34] and it has been verified that functionalized graphene are highly stable in the base fluid due to the electrostatic repulsion of the surface terminations [35]. However, to the best of our knowledge, the stabilization of functionalized graphene has never been studied in CO_2 liquid.

A new family of 2D transition metal carbides, carbonitrides, and nitrides (MXene) have recently been introduced since 2011 with the common formula of $M_{n+1}X_nT_x$ (n=1, 2, and 3) [36,37], where M is an early transition metal, X stands for carbon and/or nitrogen, and T_x

represents the surface termination (e.g., O, OH, and F). MXenes have attracted much interest due to their unusual properties and have been applied for many applications. Due to unusual properties of MXenes, many applications have experimentally been found for this new class of 2D materials such as Li ion batteries, purifiers, and catalysts [38]. Moreover, many applications have theoretically been proposed in electronics, magnetic, optical, thermoelectric, and sensing devices, as well as they have been introduced as new potential materials for catalytic and photocatalytic reactions [38]. Thus, in the present study, Ti_2CO_2 MXene is taken to be evaluated its stabilization in the CO_2 liquid. A 2D Ti_2CO_2 MXene involves trilayer sheets with a hexagonal-like unit cell, where the carbon layer is sandwiched by two titanium transition metal layers and oxygen surface terminations are attached on the surfaces. The monolayers of graphene and Ti_2CO_2 MXene are shown in **Fig. 1**.

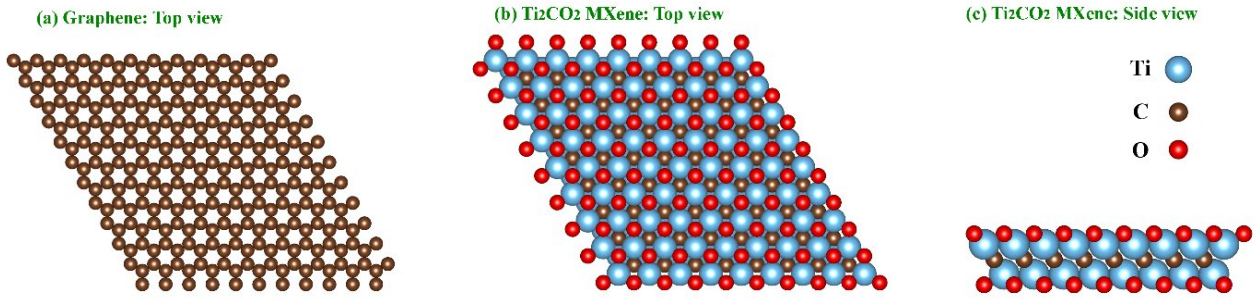

Figure 1: Nanostructures of monolayer (a) graphene (top view) and (b)-(c) Ti_2CO_2 MXene (top and side views).

Theoretical methods employed in this study are introduced in Sec. 2. We analyze and discuss the results in more detail in Sec. 3. We also provide the details of comparisons between the stabilization behaviors of different 2D nano-sheets of graphene, two-sided hydrogen-functionalized graphene (GH) and oxygen-functionalized graphene (GO) with functional group concentration of 50% as well as functionalized Ti_2CO_2 MXene. Moreover, the enhancement of the rheological properties of the CO_2 liquid based nanofluid including the corresponding nano-sheets are investigated. Conclusions are given in Sec. 4. Our findings will broaden the potential

applications of these 2D materials in producing SC-CO_2 based nanofluid, and simultaneously, provide information on how these different 2D nano-sheets disperse in SC-CO_2.

2. Computational Methodology

Atomistic modeling are performed using a Large-scale Atomic Molecular Massively Parallel Simulator (LAMMPS) molecular dynamics simulator [39–41]. Molecular modeling of SC-CO_2 fluid is challenging because of the weak intermolecular interactions. Therefore, to conduct atomistic simulations of SC-CO_2, it is essential to apply an accurate force field. Several force field potentials were proposed for atomistic modeling of SC-CO_2 in order to well capture the thermodynamic properties of the liquid [42–44]; however, some of them underestimate the inter-molecular forces and consequently the thermodynamic properties of the liquid in condensed phases. In the present study, we employ the COMPASS force field [42] as a robust and reliable force field, which can accurately model the inter-atomic and inter-molecular interactions of the CO_2 liquid, especially in condensed phases. In this force field, the total energy is calculated by contributions of bond stretching, angle deformation, cross-coupling of bond-bond and bond-angle, and non-bonded interactions including the electrostatic and van der Waals (vdW) terms. Details of the interaction parameters are given in Ref. [42]. The pure CO_2 at a super-critical condition are modeled in a simulation cell with the cell dimensions of 10 nm in each direction. The non-bonded interactions for both Van der Waals (vdW) and electrostatic forces are calculated through the charge-group-based cutoffs of 15 Å. The long-range Coulombic interactions are calculated by applying the particle-particle particle-mesh (pppm) solver [45] and the tail corrections are also included for the vdW interactions [46].

In the system including the nano-sheets as the nanoparticles in CO_2 liquid, we employ a standard 12-6 Lenard-Jones (LJ) force filed for the interaction energy calculations of the rigid sheets. The CO_2 molecules are modeled using COMPASS force field and the inter-molecular interactions between the CO_2 molecules and the sheets are modeled using arithmetic mix rule.

All other parameters for the interaction energy calculations are the same as stated for the pure CO_2 system. We note that several parameter sets are available to calculate the LJ force filed between graphene sheets [47-49]. The dependence of interaction energy on the available potential parameters were investigated [47]. Since insignificant difference was found in the trend of the interaction energy among different available parameter sets, we employ, in this study, only the parameter set of Ref. [47] in our calculations, which are listed in **Table 1**. The parameter sets of the LJ and Coulombic force fields for other nano-sheets (i.e., GH, GO, and Ti_2CO_2 MXene) are also listed in **Table 1**, which is accompanied by the corresponding references. Each functionalized nano-sheets are charge neutral. **Fig. 2** shows the schematic representation of charge distribution on the carbon atoms of the GO and GH sheets and the oxygen and hydrogen atoms of the surface terminations.

Table 1: Parameters of the classical force field employed to model nano-sheets.

Nano-sheet	Atom type	Q (e)	e (meV)	σ (Å)	Reference
Graphene	C	0.0	2.50	3.37	Ref. [47]
GH	C H	-0.115 0.115	4.7266 0.6938	3.4 2.5	Ref. [32]
GO	C O	0.18 -0.36	6.7366 6.7366	3.166 3.5532	Ref. [48,49]
Ti_2CO_2 MXene	Ti C O	1.5546 -1.3092 -0.90	6.7366 6.7366 6.7366	3.166 3.166 3.5532	Ref. [49]

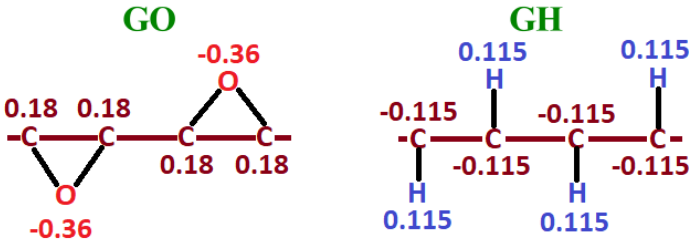

Figure 2: Schematic of partial charge assignment of covalently functionalized GO and GH nano-sheets.

The lattice parameter of the corresponding hexagonal unit cells are almost 0.31 nm. A 8×8×1 supercell of the monolayers are made (see **Fig. 1**) so that the hexagonal nano-sheets with the lattice parameter of almost 2.5 nm are placed inside the simulation box with the size of 7.5 nm in all directions, which is filled with very nearly 4000 CO_2 molecules. In this study, five nano-

sheets are immersed in the liquid CO_2 for the systems consist of graphene, GH, and GO. Since Ti_2CO_2 MXene is thicker than graphene (see **Fig. 1**), only three nano-sheets are modeled for the system consist of Ti_2CO_2 MXene to provide almost the same volume fraction of the nanoparticles.

Verlet integration [50] with a 0.2 fs time step is employed to integrate Newton's equations of motions for all the systems. In order to provide the super-critical condition, we, first, pre-equilibrate the systems at 380 K for 0.2 ns by applying the isothermal NVT canonical ensemble for all the system of atoms initially arranged in a perfect structure lattice. Second, the isothermal-isobaric NPT ensemble are performed for 1.6 ns to achieve the temperature of 380 K and pressure of 200 bar. Then, the densities and thermo-physical properties (i.e., viscosity and self-diffusion) of the systems are calculated by averaging over 0.5 ns trajectory.

We use Green-kubos (GK) relations [51,52] to calculate the shearing viscosity of the system, which give the exact mathematical expression for the stress autocorrelation function (SAFC; $C_\eta(t)$) in terms of time correlation functions:

$$C_\eta(t) = \langle \sum_{x<y} P_{xy}(t) P_{xy}(0) \rangle \quad (1)$$

P_{xy} denotes an independent component of the stress in the xy-direction. Other off-diagonal P_{xz} and P_{yz} components of the stress tensor are also calculated for the shear viscosity calculation. The brackets <. . .> represent an average over an equilibrium ensemble. Then, the viscosity is calculated by the SAFC integration over time:

$$\eta = \frac{V}{K_B T} \int_0^\infty C_\eta(t) dt \quad (2)$$

where η is the viscosity and V, T, and K_B are the volume of the system, temperature in Kelvin, and the Boltzmann constant, respectively.

We use the Einstein relation[53] for the calculation of self-diffusion coefficient (D):

$$D = \frac{1}{6} \lim_{t \to \infty} \frac{d}{dt} \langle (r_i(t) - r_i(0))^2 \rangle \quad (3)$$

where $r_i(t)$ is the position of the center of mass of atom *i* at time *t*, $r_i(0)$ is the initial position of the atom, and $<(r_i(t) - r_i(0))^2>$ refers to an ensemble average, representing the mean square displacement (MSD). The self-diffusion coefficient of the diffusing atoms in a canonical ensemble is obtained by fitting the slope of the calculated MSD over the averaging period. It is worth noting that the system-size could affect the calculated self-diffusion coefficient. In the present study, we examined the system-size effects on the accuracy of the self-diffusion coefficient the results showed that the system-size considered is large enough to avoid affecting the self-diffusion coefficient calculation.

3. Results and Discussion

In order to study the rheological properties of the CO_2 based nanofluid containing the corresponding nano-sheets as well as the stabilization of those nano-sheets in the CO_2 fluid at super-critical condition, we, first, focus on the modeling of pure CO_2 at the super-critical condition of 380 K and 200 bars. In our previously published study [6], we comprehensively confirmed our results of viscosity, self-diffusion, and Radial-Distribution-Function (RDF) with other theoretical and experimental results at different thermodynamic conditions. Here, however, we only compare our calculations of liquid CO_2 density and viscosity to other theoretical and experimental results in **Table 2** in order to provide a validation for the computational methodology employed with the force filed potentials selected in this study. The value of calculated density (0.459 g/cm^3) is well matched with the experimental result of Ref. [54] (0.449 g/cm^3), while our calculated viscosity (0.029 cP) has a small deviation with the theoretical result of Ref. [55] (0.035 cP). This small deviation was generally observed for the viscosity calculation by atomistic-scale modeling. The main source of the deviation is attributed to the time correlations between the stress tensors at varying time intervals and time integration of the correlation data over a long time.

Table 2. SC-CO_2 density and viscosity calculated in the present study at T = 380 K and P = 200 bar. Other theoretical and experimental results are also stated for comparison.

	Present study	Previous studies
Density (g/cm^3)	0.459	0.449 – (Ref. [54])
Viscosity (cP)	0.029	0.035 – (Ref. [55])

After endorsing our computational methodology by comparing the rheological properties of pure CO_2 liquid at the corresponding super-critical thermodynamic condition with the available data, we, next, investigate the stability and the rheological properties of CO_2 liquid based nanofluid including different 2D nano-sheets at the same thermodynamic condition of 380 K and 200 bars.

We separately immerse five nano-sheets of graphene, GH, and GO as well as three nano-sheets of Ti_2CO_2 MXene in the liquid with a distance of almost 12.0 Å to make the nanofluid with volume fraction of almost 2%. **Fig. 3** shows the snapshot results of stabilization of different nano-sheets over 2.3 ns of modeling. Our results generally show that pristine graphene and Ti_2CO_2 MXene nano-sheets aggregate firmly over time while functionalized graphene attach together from their edges.

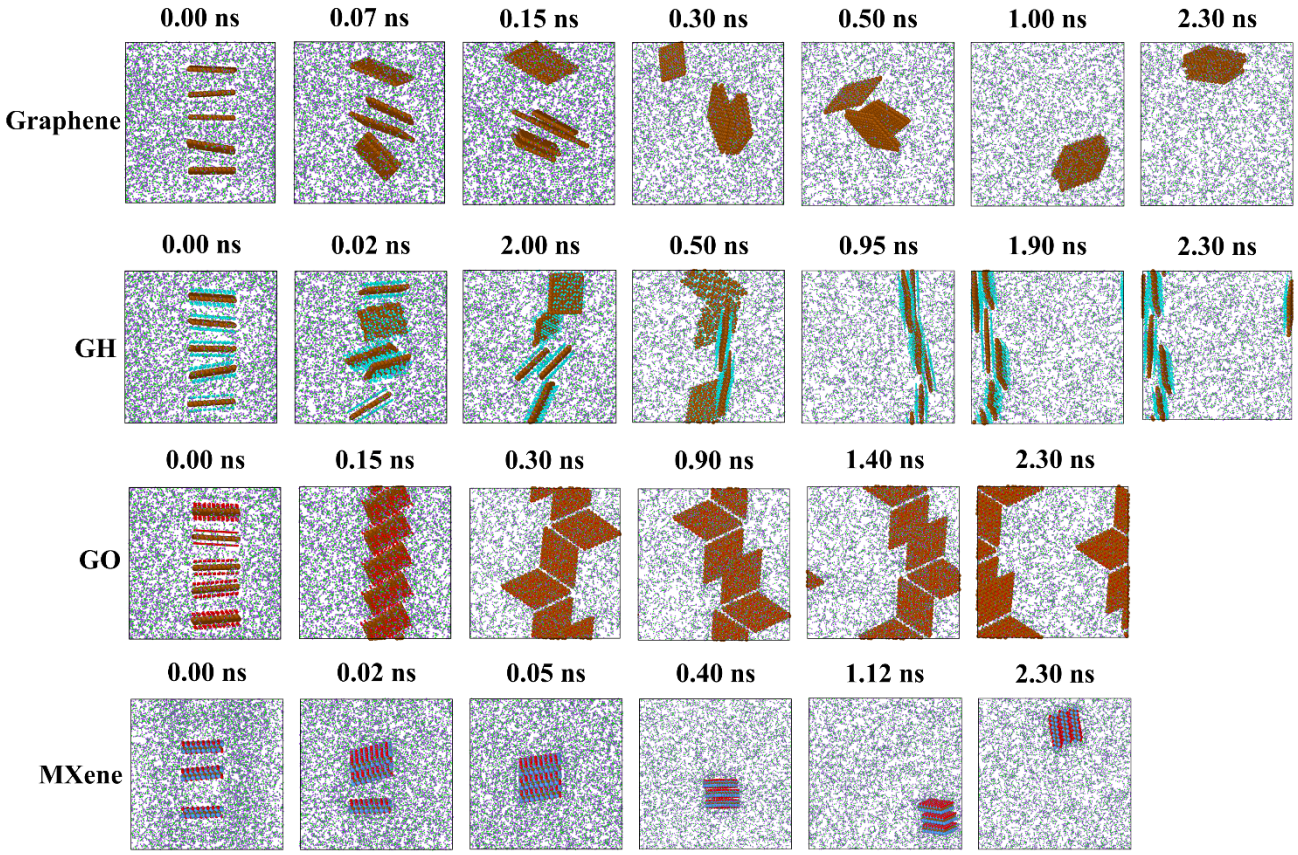

Figure 3: Snapshot results of stabilization of different 2D nano-sheets immersed in CO_2 liquid.

In the case of nanofluid containing pristine graphene, the results show that there are favorable interactions between the nano-sheet surfaces so that they start aggregation steadily and all the nano-sheets stick together after 1.0 ns, as shown in **Fig. 3**. We also calculate the average distance between the center of upper and lower nano-sheets over 0.5 ns (**Fig. 4**) to highlight more significantly the dispersion behavior of different nano-sheets in the CO_2 liquid. It is illustrated that the average distance is continually reduced after 0.2 ns. Since the RDF would provide the information about the aggregation and diffusion status of the system, we also calculate the intermolecular pair correlation functions for C–C of the nano-sheets and CO_2 molecules for the SC-CO_2 based nanofluid including different nano-sheets (see **Fig. 5a**). The accumulation of CO_2 molecules around different nano-sheets at the end of simulation is also shown in **Fig. 5b**. Our results clearly illustrate that the aggregation of the CO_2 molecules around the pristine graphene is lower than other nano-sheets. Our results indicate that the adsorbed CO_2 molecules on the graphene surfaces could not afford an enough repulsive barrier to prevent the aggregation of pristine graphene sheets.

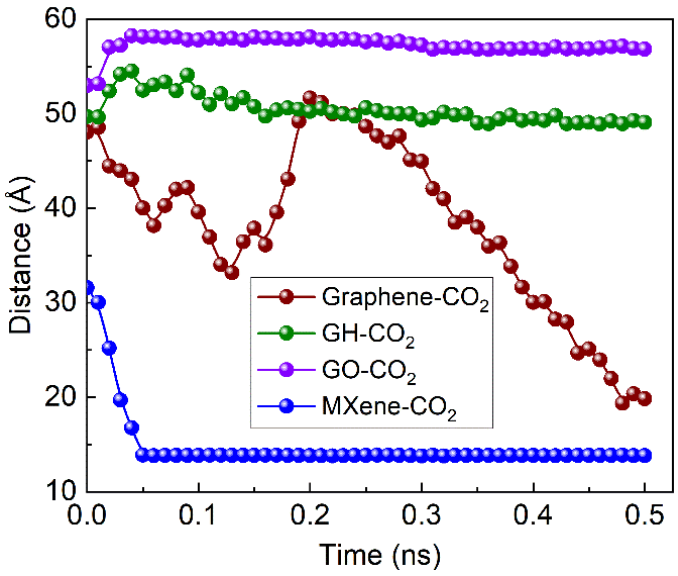

Figure 4: Calculated average distance of upper and lower nano-sheets over 0.5 ns.

Unlike pristine graphene, the results show a better stabilization for the functionalized graphene, which is attributed to the electrostatic repulsion of the functional groups. As stated in Sec. 2 (see **Table 1** and **Fig. 1**), the charges of the hydrogen and oxygen surface terminations are 0.115*e* and -0.36*e*, respectively. The calculated average distance between the center of upper and lower nano-sheets in **Fig. 4** demonstrates that both functionalized graphene have almost a similar dispersion behavior in CO_2 liquid at the corresponding super-critical condition. The nano-sheets of both functionalized graphene repel each other and this repulsion is more significant between oxygen-functionalized graphene than hydrogen-functionalized graphene. It can also be seen in snapshot results in **Fig. 3**. It could be inferred to the negative charge of the oxygen surface terminations while the charge of the hydrogen surface terminations is positive and one third of the charge of the oxygen surface terminations. The greater value of the oxygen surface charge causes a higher electrostatic repulsion between the nano-sheets compared to the hydrogen surface terminations. The calculated RDF for C–C of the nano-sheets and CO_2 molecules in **Fig. 5** illustrates that the CO_2 molecules adsorb more significantly on GO nano-sheets than GH nano-sheets, which it also provides a better repulsive barrier for GO nano-sheets to avoid the aggregation compared to GH nano-sheets. It is worth noting that the interesting stabilization performance of functionalized graphene could significantly depend on the degree of graphene functionalization. Although, in the present study, we evaluate the stabilization of functionalized graphene with 50% coverage ratio, it would be interesting to see the effect of different coverage ratios on the stabilization properties in the future study.

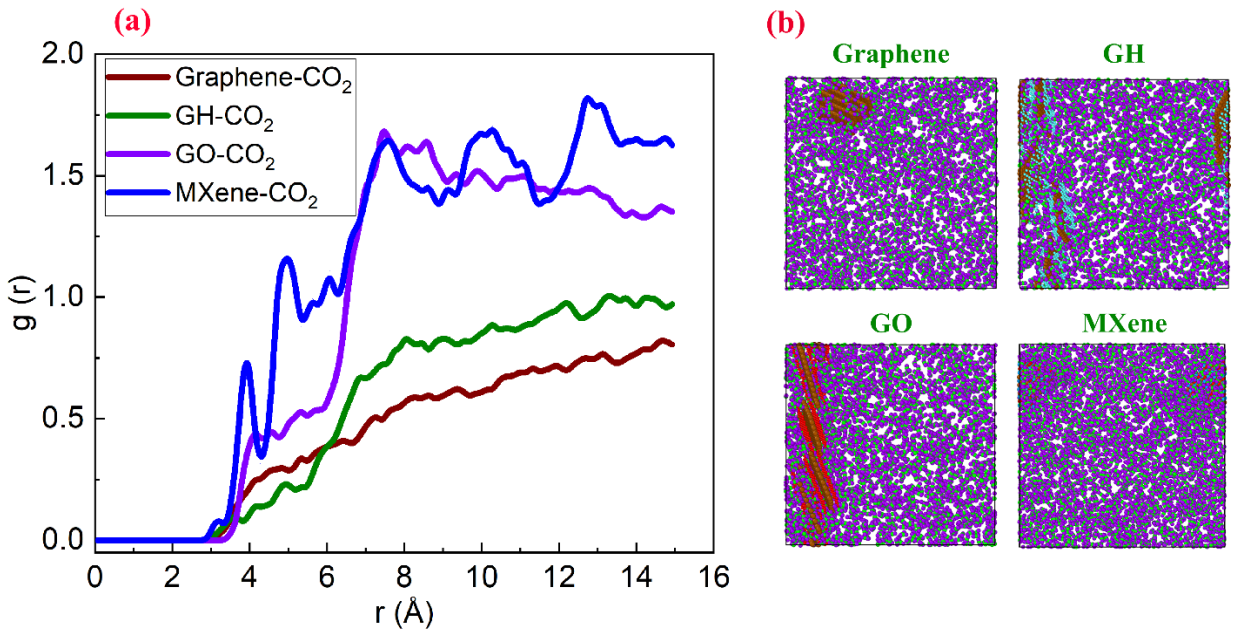

Figure 5: (a) Radial distribution function for C–C of the nano-sheets and CO_2 molecules for the SC-CO_2 based nanofluid including different nano-sheets, (b) Schematic of accumulation of CO_2 molecules around different nano-sheets at the end of simulation.

The stabilization of Ti_2CO_2 MXene in CO_2 liquid proves a strong binding between the nano-sheets despite the existence of oxygen surface functional groups. Snapshot results in **Fig. 3** illustrates that the MXene nano-sheets bind together in 0.05 ns. This is also clearly presented in **Fig. 4** that the distance between the center of upper and lower carbon planes is continually decreasing during 0.05 ns, where all three nano-sheets stick together and never separate until the end of the simulation time. Although the MXene nano-sheets are covered by oxygen surface terminations, the electrostatic repulsion of the corresponding functional groups cannot provide adequate repulsive barrier to avoid aggregating the MXene nano-sheets. It can be recognized that the interlayer coupling between each MXene nano-sheet is stronger than electrostatic repulsions. Comparing to the pristine graphene, our results show that the van der Waals coupling between the pristine graphene is much weaker than Ti_2CO_2 MXene, where functionalized graphene could provide enough repulsive forces for the stabilization of GO and GH while oxygen surface terminations in MXene could not provide such this enough repulsion.

Our calculated results of RDF for C–C of the nano-sheets and CO_2 molecules in **Fig. 5** show that the accumulation of CO_2 molecules around the Ti_2CO_2 MXene is much higher than the pristine graphene and GH while it is marginally higher than GO. The results could be attributed to the existence of oxygen surface termination with negative charges so that they can attract more CO_2 molecules. Even though the Ti_2CO_2 MXene has a strong capability to attract the CO_2 molecules, it could not hinder the aggregation of the nano-sheets due to the strong interlayer coupling. By comparing the stabilization of all different nano-sheets in CO_2 liquid, it is understood that the interlayer interaction between the MXene nano-sheets are significantly stronger than that between graphene nano-sheets with weak van der Waals interaction. This is because the functional groups in graphene could afford enough repulsion between the nano-sheets and improve the stabilization while the oxygen surface terminations in MXene could not overcome the interlayer binding between the nano-sheets. Based on our results, the stabilization of the corresponding 2D nano-sheets in CO_2 liquid are in the order of: GO > GH > pristine graphene > Ti_2CO_2 MXene.

After discussing the stabilization of the nano-sheets, the calculated results of the rheological properties (i.e., viscosity and self-diffusion) of the SC-CO_2 with those nano-sheets are evaluated. We calculate these properties using **Eqs. 2** and **3**. The calculated MSD as a function of time are fitted to obtain the self-diffusion coefficients of the CO_2 based nanofluid with different nano-sheets, as shown in **Fig. 6a**. Then, we normalize the calculated properties with those of the pure CO_2 liquid in order to have a more clear comparison between different nanofluids. The obtained normalized values of self-diffusion and viscosity are shown in **Fig. 6b**. The results show that GO nano-sheets enhance the viscosity of the nanofluid more than other nano-sheets. By comparison of all three graphene, GH, and GO nano-sheets, it could be understood that immersing the nano-sheets in the CO_2 liquid provide a greater viscosity enhancement as much as they could disperse in the CO_2 liquid. The results of the normalized

self-diffusion also illustrate that the migration of CO_2 molecules within the system are more hardened in more stable nanofluid, as we expected based on the Stokes-Einstein equation[56].

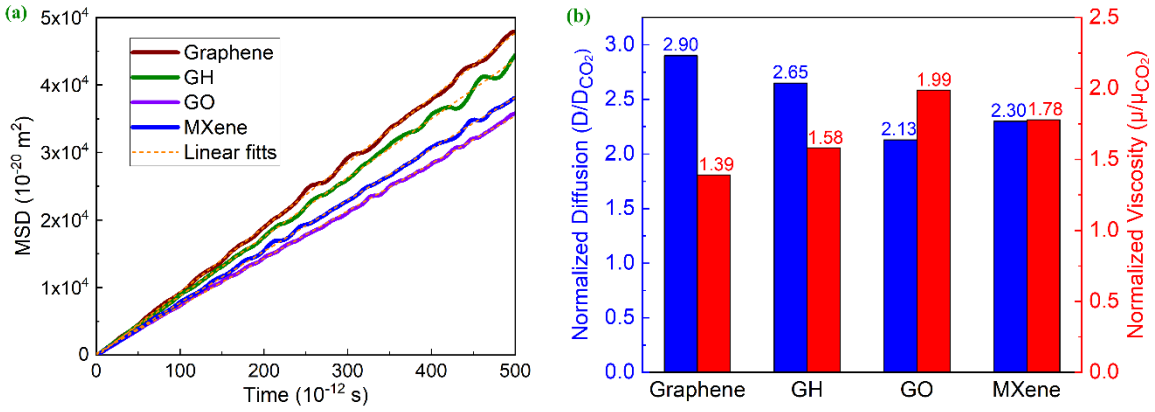

Figure 6: (a): MSD results and their linear fits over the averaging period for the self-diffusion coefficient calculations, and (b) Normalized self-diffusion coefficient (blue bars) and normalized viscosity (red bars) of the CO_2 based nanofluid for with different nano-sheets.

The result of the calculated normalized viscosity for the nanofluid including Ti_2CO_2 MXene show although the stabilization of the MXene nano-sheets in the CO_2 liquid is very poor, they could have a better impact on the viscosity enhancement compare to pristine graphene and GH nano-sheets. It could be attributed to the volume fraction of the nano-sheets, which affect significantly the nanofluid viscosity. Since the MXene nano-sheets accumulate a larger number of CO_2 molecules around themselves, the final volume fraction of MXene nano-sheets is higher than other nano-sheets. The comparison of MXene nano-sheets and GO would be more reasonable since they provide a similar volume fraction. As can be seen in **Fig. 6b**, GO nano-sheets have a superior impact on the viscosity enhancement of the CO_2 based nanofluid since they are more stabilized.

4. Conclusion

We employed Molecular Dynamics (MD) modeling to explore the stabilization of 2D graphene, GH, GO, and Ti_2CO_2 MXene nano-sheets in SC-CO_2 liquid as well as the rheological properties of the nanofluid with the corresponding nano-sheets. Our results showed that the MXene nano-sheets with the presence of the oxygen surface terminations aggregate in the CO_2

liquid faster than the pristine graphene. Although the oxygen surface terminations of the MXene could attract more CO_2 molecules compare to the pristine graphene, the accumulated CO_2 molecules around the MXene nano-sheets could not provide enough sufficient repulsive forces to avoid the aggregation of MXene nano-sheets. It was attributed to the stronger interlayer coupling between the MXene nano-sheets than the pristine graphene nano-sheets. However, the weaker interlayer coupling between the pristine graphene nano-sheets can be overcome by the repulsive forces induced by the surface functionalization, which can significantly improve the stability of the graphene in the CO_2 liquid. The stabilization of graphene was more improved by oxygen functional groups than hydrogen functional groups since oxygen functional groups could provide larger repulsive forces between the nano-sheets and could also attract more CO_2 molecules on the surfaces inducing extra repulsion. The stability of the corresponding nano-sheets in the SC-CO_2 followed the sequence GO > GH > graphene > Ti_2CO_2 MXene. Our calculated rheological properties of the nanofluids including different nano-sheets exhibited that immersing the nano-sheets with the same volume fraction in the CO_2 liquid provide a higher viscosity enhancement as much as they could stabilize in the liquid.

Acknowledgment

The authors would like to acknowledge and greatly appreciate the financial support from VISTA which is a basic research program in collaboration between the Norwegian Academy of Science and Letters, and Statoil. The authors would also like to thank Department of Mechanical and Industrial Engineering at Norwegian University of Science and Technology (NTNU). The authors also acknowledge generous grants of high performance computer time from both Vilje and UNINETT Sigma.

References

1 S. Qiu, Z. Zhou, J. Dong and G. Chen, Preparation of Ni Nanoparticles and Evaluation of Their Tribological Performance as Potential Additives in Oils, *J. Tribol.*, 2007, **123**, 441.

2 B. Li, X. Wang, W. Liu and Q. Xue, Tribochemistry and antiwear mechanism of organic-inorganic nanoparticles as lubricant additives, *Tribol. Lett.*, 2006, **22**, 79–84.

3 L. Rapoport, V. Leshchinsky, I. Lapsker, Y. Volovik, O. Nepomnyashchy, M. Lvovsky, R. Popovitz-Biro, Y. Feldman and R. Tenne, Tribological properties of WS2 nanoparticles under mixed lubrication, *Wear*, 2003, **255**, 785–793.

4 L. Rapoport, V. Leshchinsky, M. Lvovsky, I. Lapsker, Y. Volovik, Y. Feldman, R. Popovitz-Biro and R. Tenne, Superior tribological properties of powder materials with solid lubricant nanoparticles, *Wear*, 2003, **255**, 794–800.

5 B. Wei, Q. Li, F. Jin, H. Li and C. Wang, The Potential of a Novel Nanofluid in Enhancing Oil Recovery, *Energy and Fuels*, 2016, **30**, 2882–2891.

6 R. Khaledialidusti, A. K. Mishra and A. Barnoush, Rheological properties of super critical CO2 with CuO: Multi-scale computational modeling, *J. Chem. Phys.*, , DOI:10.1063/1.5053571.

7 B. Venkateswarlu and P. V. Satya Narayana, Chemical reaction and radiation absorption effects on the flow and heat transfer of a nanofluid in a rotating system, *Appl. Nanosci.*, 2015, **5**, 351–360.

8 A. Loya and G. Ren, Molecular dynamics simulation study of rheological properties of CuO–water nanofluid, *J. Mater. Sci.*, 2015, **50**, 4075–4082.

9 P. C. Mishra, S. Mukherjee, S. K. Nayak and A. Panda, A brief review on viscosity of nanofluids, *Int. Nano Lett.*, 2014, **4**, 109–120.

10 S. Zhang and X. Han, Effect of different surface modified nanoparticles on viscosity of nanofluids, *Adv. Mech. Eng.*, 2018, **10**, 1–8.

11 J. Garg, B. Poudel, M. Chiesa, J. B. Gordon, J. J. Ma, J. B. Wang, Z. F. Ren, Y. T. Kang, H. Ohtani, J. Nanda, G. H. McKinley and G. Chen, Enhanced thermal conductivity and viscosity of copper nanoparticles in ethylene glycol nanofluid, *J. Appl. Phys.*, , DOI:10.1063/1.2902483.

12 L. S. Sundar, M. K. Singh, E. V. Ramana, B. Singh, J. Grácio and A. C. M. Sousa, Enhanced Thermal Conductivity and Viscosity of Nanodiamond-Nickel Nanocomposite Nanofluids, *Sci. Rep.*, 2014, **4**, 1–14.

13 F. Duan, T. F. Wong and A. Crivoi, Dynamic viscosity measurement in non-Newtonian graphite nanofluids, *Nanoscale Res. Lett.*, 2012, **7**, 1–15.

14 A. Wilson, Experimental and Numerical Studies of CO2 EOR in Unconventional Reservoirs SPE Hydraulic Fracturing Technology Conference, *J. Pet. Technol.*, 2017, 11–13.

15 F. M. Al-Otaibi, X. Zhou and S. L. Kokal, Laboratory Evaluation of Different Modes of Supercritical Carbon Dioxide Miscible Flooding for Carbonate Rocks, *SPE Reserv. Eval. Eng.*, 2018, **22**, 137–149.

16 C. Carpenter, Experimental Program Investigates Miscible CO_2 WAG Injection in Carbonate Reservoirs, *J. Pet. Technol.*, 2018, **71**, 47–49.

17 K. Jessen and E. H. Stenby, Fluid Characterization for Miscible EOR Projects and CO2 Sequestration, *SPE Reserv. Eval. Eng.*, 2007, **10**, 482–488.

18 C. Carpenter, Integrated CO_2-Foam Pilot in a Heterogeneous Carbonate Field, *J. Pet. Technol.*, 2018, **70**, 72–74.

19 M. I. Kuhlman, Visualizing the Effect of Light Oil on CO2 Foams, 1990, Society of Petroleum Engineers. doi:10.2118/17356-PA.

20 H. O. Lee, J. P. Heller and P. Recovery, Laboratory Measurements of CO2 -Foam Mobility, 1990, 193–197.

21 C. Carpenter, CO_2-Foam Field Pilot Test in a Sandstone Reservoir, *J. Pet. Technol.*,

2018, **70**, 70–71.

22 D. Ortiz, M. Izadi and S. I. Kam, Modeling of Nanoparticle-Stabilized CO_2 Foam Enhanced Oil Recovery, *SPE Reserv. Eval. Eng.*, 2019, 1–19.

23 C. Carpenter, Gelled Emulsions of CO2, Water, and Nanoparticles, *J. Pet. Technol.*, 2015, **66**, 135–137.

24 A. S. Emrani and H. A. Nasr-El-Din, Stabilizing CO_2 Foam by Use of Nanoparticles, *SPE J.*, 2017, **22**, 494–504.

25 H. Zhang, J. W. Huang, J. Velasco, K. Myhro, M. Maldonado, D. D. Tran, Z. Zhao, F. Wang, Y. Lee, G. Liu, W. Bao and C. N. Lau, Transport in suspended monolayer and bilayer graphene under strain: A new platform for material studies, *Carbon N. Y.*, 2014, **69**, 336–341.

26 A. K. Geim, Graphene : Status and Prospects, 2010, **1530**, 1530–1535.

27 P. Article, The rise of graphene-nature mater.pdf, 2007, 183–191.

28 L. Tsetseris and S. T. Pantelides, Graphene: An impermeable or selectively permeable membrane for atomic species?, *Carbon N. Y.*, 2014, **67**, 58–63.

29 B. J. Hong, O. C. Compton, Z. An, I. Eryazici and S. T. Nguyen, Successful stabilization of graphene oxide in electrolyte solutions: Enhancement of biofunctionalization and cellular uptake, *ACS Nano*, 2012, **6**, 63–73.

30 S. Pei and H. M. Cheng, The reduction of graphene oxide, *Carbon N. Y.*, 2012, **50**, 3210–3228.

31 J. Azamat, Functionalized Graphene Nanosheet as a Membrane for Water Desalination Using Applied Electric Fields: Insights from Molecular Dynamics Simulations, *J. Phys. Chem. C*, 2016, **120**, 23883–23891.

32 J. Azamat, A. Khataee and S. W. Joo, Molecular dynamics simulation of trihalomethanes separation from water by functionalized nanoporous graphene under induced pressure, *Chem. Eng. Sci.*, 2015, **127**, 285–292.

33 Y. Tan, L. Wang, J. Xiao, X. Zhang, Y. Wang, C. Liu, H. Zhang, C. Liu, Y. Xia and K. Sui, Synchronous enhancement and stabilization of graphene oxide liquid crystals: Inductive effect of sodium alginates in different concentration zones, *Polymer (Guildf).*, 2019, **160**, 107–114.

34 D. Parviz, S. Das, H. S. T. Ahmed, F. Irin, S. Bhattacharia and M. J. Green, Dispersions of non-covalently functionalized graphene with minimal stabilizer, *ACS Nano*, 2012, **6**, 8857–8867.

35 C. N. Yeh, K. Raidongia, J. Shao, Q. H. Yang and J. Huang, On the origin of the stability of graphene oxide membranes in water, *Nat. Chem.*, , DOI:10.1038/nchem.2145.

36 M. Naguib, M. Kurtoglu, V. Presser, J. Lu, J. Niu, M. Heon, L. Hultman, Y. Gogotsi and M. W. Barsoum, Two-dimensional nanocrystals produced by exfoliation of Ti 3AlC 2, *Adv. Mater.*, 2011, **23**, 4248–4253.

37 M. Naguib, O. Mashtalir, J. Carle, V. Presser, J. Lu, L. Hultman, Y. Gogotsi and M. W. Barsoum, Two-dimensional transition metal carbides., *ACS Nano*, 2012, **6**, 1322–31.

38 B. Anasori, M. R. Lukatskaya and Y. Gogotsi, 2D metal carbides and nitrides

(MXenes) for energy storage, *Nat. Rev. Mater.*, , DOI:10.1038/natrevmats.2016.98.

39 S. Plimpton and others, LAMMPS-large-scale atomic/molecular massively parallel simulator, *Sandia Natl. Lab.*

40 S. Plimpton, P. Crozier and A. Thompson, LAMMPS-large-scale atomic/molecular massively parallel simulator. 2007, 18, 43-43, *Sandia Natl. Lab.*, , DOI:10.1002/ejoc.201200111.

41 S. Plimpton, Plimpton1995.Pdf, *J. Comput. Phys.*, , DOI:10.1006/jcph.1995.1039.

42 J. Yang, Y. Ren, A. Tian and H. Sun, COMPASS Force Field for 14 Inorganic Molecules, He, Ne, Ar, Kr, Xe, H2 , O2 , N2 , NO, CO, CO2 , NO2 , CS2 , and SO2, in Liquid Phases , *J. Phys. Chem. B*, 2002, **104**, 4951–4957.

43 Z. Zhang and Z. Duan, An optimized molecular potential for carbon dioxide, *J. Chem. Phys.*, , DOI:10.1063/1.1924700.

44 J. G. Harris and K. H. Yung, Carbon dioxide's liquid-vapor coexistence curve and critical properties as predicted by a simple molecular model, *J. Phys. Chem.*, 1995, **99**, 12021–12024.

45 R. W. Hockney and J. W. Eastwood, *Computer Simulation Using Particles*, 1989.

46 H. Sun, COMPASS: An ab Initio Force-Field Optimized for Condensed-Phase ApplicationsOverview with Details on Alkane and Benzene Compounds, *J. Phys. Chem. B*, 2002, **102**, 7338–7364.

47 Y. Shibuta and S. Maruyama, Molecular dynamics simulation of formation process of single-walled carbon nanotubes by CCVD method, *Chem. Phys. Lett.*, 2003, **382**, 381–386.

48 A. J. P. Neto, V. V. Chaban and E. E. Fileti, Hydration peculiarities of graphene oxides with multiple oxidation degrees, *Phys. Chem. Chem. Phys.*, 2017, **19**, 32333–32340.

49 E. S. Muckley, M. Naguib, H. W. Wang, L. Vlcek, N. C. Osti, R. L. Sacci, X. Sang, R. R. Unocic, Y. Xie, M. Tyagi, E. Mamontov, K. L. Page, P. R. C. Kent, J. Nanda and I. N. Ivanov, Multimodality of Structural, Electrical, and Gravimetric Responses of Intercalated MXenes to Water, *ACS Nano*, 2017, **11**, 11118–11126.

50 L. Verlet, Computer 'Experiments' on Classical Fluids. I. Thermodynamical Properties of Lennard-Jones Molecules, *Phys. Rev.*, 1967, **159**, 183–195.

51 M. S. Green, Markoff random processes and the statistical mechanics of time-dependent phenomena. II. Irreversible processes in fluids, *J. Chem. Phys.*, 1954, **22**, 398–413.

52 R. Kubo, M. Yokota and S. Nakajima, Statistical-Mechanical Theory of Irreversible Processes. Response to Thermal Disturbance, *J. Phys. Soc. Japan*, 1957, **12**, 1203–1211.

53 MP. Allen and DJ. Tildesley, Computer simulation of liquids. Oxford university press, 2017.

54 R. Span and W. Wagner, A new equation of state for carbon dioxide covering the fluid region from the triple-point temperature to 1100 K at pressures up to 800 MPa, *J. Phys. Chem. Ref. Data*, , DOI:10.1063/1.555991.

55 A. F. and W. A. Wakeham, The Viscosity of Carbon Dioxide, *Proc. R. Soc. A Math. Phys. Eng. Sci.*, 1998, **27**, 31–44.

56 E. Albert, Investigations on the Theory of the Brownian Movement. Courier Corporation, 1956.